Reflectance Speckle of Retinal Nerve Fiber Layer Reveals Axonal Activity

Xiang-Run Huang,[1,2] Robert W. Knighton,[1] Ye Zhou,[2] and Xiao-Peng Zhao[1]

[1]Bascom Palmer Eye Institute, University of Miami, Miami, Florida
[2]Department of Biomedical Engineering, University of Miami, Miami, Florida

Correspondence: Xiang-Run Huang, Bascom Palmer Eye Institute, University of Miami Miller School of Medicine, 1638 NW Tenth Avenue, Miami, FL 33136; xhuang3@med.miami.edu.

Submitted: November 21, 2012
Accepted: March 13, 2013

Citation: Huang X-R, Knighton RW, Zhou Y, Zhao X-P. Reflectance speckle of retinal nerve fiber layer reveals axonal activity. *Invest Ophthalmol Vis Sci*. 2013;54:2616–2623. DOI:10.1167/iovs.12-11347

Purpose. This study investigated the retinal nerve fiber layer (RNFL) reflectance speckle and tested the hypothesis that temporal change of RNFL speckle reveals axonal dynamic activity.

Methods. RNFL reflectance speckle of isolated rat retinas was studied with monochromatic illumination. A series of reflectance images was collected every 5 seconds for approximately 15 minutes. Correlation coefficients (CC) of selected areas between a reference and subsequent images were calculated and plotted as a function of the time intervals between images. An exponential function fit to the time course was used to evaluate temporal change of speckle pattern. To relate temporal change of speckle to axonal activity, in vitro living retina perfused at a normal (34°C) and a lower (24°C) temperature, paraformaldehyde-fixed retina, and retina treated with microtubule depolymerization were used.

Results. RNFL reflectance was not uniform; rather nerve fiber bundles had a speckled texture that changed with time. In normally perfused retina, the time constant of the CC change was 0.56 ± 0.26 minutes. In retinas treated with lower temperature and microtubule depolymerization, the time constants increased by two to four times, indicating that the speckle pattern changed more slowly. The speckled texture in fixed retina was stationary.

Conclusions. Fixation stops axonal activity; treatments with either lower temperature or microtubule depolymerization are known to decrease axonal transport. The results obtained in this study suggest that temporal change of RNFL speckle reveals structural change due to axonal activity. Assessment of RNFL reflectance speckle may offer a new means of evaluating axonal function.

Keywords: RNFL reflectance, speckle, axonal transport, coherence

Glaucoma and other optic nerve diseases cause visual loss by damaging the retinal nerve fiber layer (RNFL), which consists of axons of retinal ganglion cells. Because recognizable loss of the RNFL may precede measurable loss of vision, various optical methods, such as optical coherence tomography (OCT), scanning laser polarimetry (SLP), and confocal scanning laser ophthalmoscopy (cSLO), have been developed to aid the diagnosis and management of the disease.[1–3] Often these methods assess the RNFL structure by measuring its optical properties. For example, SLP measures the retardance of the RNFL; decrease of RNFL retardance suggests loss of microtubules.[4–7] The high reflectance of normal RNFL allows OCT and cSLO to measure RNFL thickness. Recent reports also suggest that RNFL reflectance decreases in glaucomatous retinas, perhaps from damage to the axonal cytoskeleton.[8–11] Until now, measurements of the optical properties have been implemented with static imaging of the RNFL. In this report, we introduce a new concept for optical assessment of the RNFL, that is, assessment of axonal dynamic activity by observing the temporal change of RNFL reflectance speckle.

Speckle arises from interference of coherent light scattering from different parts of an object.[12–14] Speckle contrast is appreciable when the difference of the optical paths of scattered light is less than the coherence length of the incident beam. Speckle produced from biological materials is called bio-speckle. In biological tissue imaging, speckle is often considered as a source of noise due to its apparent degradation of image quality.[13] On the other hand, movement of scattering particles within tissues causes fluctuations in interference and thus changes the interference pattern, producing temporal and spatial variations in the speckle pattern.[12–14] The temporal change of bio-speckle can provide information about the physiological activity of living tissues; for instance, flowmetry based on temporal change of speckle has been developed to measure blood flow.[12,15–18]

In an earlier study with coherent illumination and high resolution imaging, RNFL reflectance speckle was observed and the speckle pattern was noted to change with time.[19] In that study, however, the speckle phenomena were considered as a source contributing to measurement variability of existing optical methods. In fact, axons are dynamic structures; they bi-directionally transport molecules, vesicles, and organelles to achieve communication between the ganglion cell bodies and their terminal targets.[20–23] To the extent that the movement of these cellular components affects the reflecting structures, this dynamic activity should induce change in the RNFL reflectance speckle. It is plausible, therefore, that the previously observed temporal change in RNFL reflectance speckle reveals dynamic activity in axons. In this study, we explored the temporal change of RNFL reflectance speckle and tested the hypothesis that temporal change of RNFL reflectance speckle is associated with axonal dynamic activity.

Materials and Methods

Experimental Preparation

Rat retinas were used in this study due to the anatomic similarities of their axons with human retinas; especially, as in humans, the axons in the rat RNFL are unmyelinated and hence similarities of their optical properties are expected. Isolated retinas were used to eliminate complications of other ocular tissues, such as the cornea and lens, in studying the optical properties of RNFL. Tissue preparation followed previously developed procedures.[19] Briefly, the eye of an anesthetized rat was removed and the animal was euthanized. An eye cup of 5 mm diameter that included the optic nerve was excised with a razor blade and placed in a dish of a warm (33–35°C) oxygenated physiologic solution. Excess vitreous was drained. The retina was dissected free of the RPE and choroid and then draped across a slit in a black membrane with the photoreceptor side against the membrane. A second, thinner membrane with a slit matched to the black membrane was put on the RNFL surface to gently stretch the retina and eliminate wrinkles. The mounted retina was placed in a chamber perfused with a warm physiologic solution to maintain the tissue alive. Reflectance images were then collected to study speckle phenomena of RNFL reflectance. Detailed ingredients of the physiologic solution can be found in an earlier publication.[19]

In addition to normally prepared retinas, retinas under other physiologic conditions were also used in the experiments, including fixed retinas, retinas perfused at lower temperatures, and retinas treated with colchicine, a microtubule (MT) depolymerizing agent. The rationale for using these retinas is presented in the Results and Discussion sections. For fixed retina, a mounted retina was fixed with 3% paraformaldehyde for 30 minutes at 34°C and thoroughly rinsed with warm physiologic solution. The mounted retina was then placed in the chamber and studied with procedures identical to that for a normally prepared retina. To examine a retina at lower temperature, the temperature of the perfusion solution in the chamber was set to 24°C. For a retina treated with colchicine, an experiment consisted of a baseline period during which the chamber was perfused with a 34°C solution containing no colchicine, followed by a treatment period during which the solution was switched to a similar solution containing 10 mM colchicine.[24] The baseline and treatment periods lasted approximately 30 minutes and 60 minutes, respectively. A total of five normal retinas, six fixed retinas, three retinas treated with low temperature, and four retinas treated with colchicine were included in this study. The protocol for the use of animals was approved by the Animal Care and Use Committee of the University of Miami and procedures adhered to the Association for Research in Vision and Ophthalmology (ARVO) Statement for the Use of Animals in Ophthalmic and Vision Research.

Imaging Microreflectometry and Formation of RNFL Reflectance Speckle

The imaging microreflectometer (IMR) has been described previously.[19,25] Briefly, the retina mounted in a chamber was illuminated by a monochromatic light source that used a tungsten-halogen lamp and interference filters. Filters were available for wavelengths ranging from 400 nm to 830 nm, with 10 nm bandwith at half-height. The retina was imaged by a camera consisting of an objective lens (f-number = 3.6) and a cooled charge-coupled device (CCD, U47+ Digital Imaging System; Apogee Instruments, Inc., Logan, UT). The optical axes of the camera and light source coincided with radii of a spherical coordinate system centered on the retina. The camera could be moved in azimuth with the elevation fixed at 13° below the equator, and the light source could be adjusted both in azimuth and elevation.

The CCD chip had 1024×1024 pixels with each pixel size of 13×13 μm. The camera provided a magnification of ×6 in air and had a full field of view of 2.3×2.3 mm with a digital resolution of 2.2 μm/pixel. Speckle size at the sensor, which solely depends on an imaging system, was calculated as[14]

$$S = 2.44\,\lambda\,(1 + M)\,F \qquad (1)$$

where λ is the illumination wavelength, M is the camera's magnification in air, and F is the f-number of the objective lens. For λ at 660 nm, the IMR provided a speckle size of 41 μm at the sensor and 7 μm at the image plane in air. Thus, one speckle was approximately 3 pixels wide in an image.

Although the incandescent light source of our IMR was not inherently coherent, the addition of a monochromatic filter introduced coherence, mainly temporal coherence with negligible spatial coherence.[26] At any given point, there was a coherence volume from within which scattered rays could interfere. The volume of coherence was approximated as a cylinder with the height determined by the coherence length (L) of the light source calculated as

$$L = \frac{2\ln(2)}{\pi n}\frac{\lambda^2}{\Delta\lambda} \qquad (2)$$

where $n = 1.35$ for the refractive index of the retina and $\Delta\lambda =$ 10 nm, the bandwidth of the filters used in the IMR. The diameter of the coherence disc was calculated as

$$d \approx 0.16\lambda/\alpha, \qquad (3)$$

with the divergence angle of the illumination beam $\alpha = 2.86°$ in the IMR.[27]

Measurement of RNFL Reflectance

To study RNFL reflectance speckle, reflectance images of isolated retinas were collected. In experiments, nerve fiber bundles were oriented approximately vertically, and the camera and light source were adjusted to positions that gave maximum (on-peak) reflectance of the nerve fiber bundles, with a dark and uniform background.[28] A series of reflectance images at 660 nm were collected every 5 seconds for approximately 15 minutes. Exposure duration was 2 seconds, which ensured no saturation occurred in any images. Black images taken with the same exposure duration, but with the light source off, were subtracted from each image, to compensate for the dark current and bias level of the CCD. The resulting pixel values were then directly proportional to the reflected intensity.

Analysis of RNFL Reflectance Speckle

Speckles are a random pattern of interference fringes; in RNFL reflectance images, speckles appear as clusters of bright and dark pixels with sizes given by Equation 1. To analyze dynamic change of RNFL speckle, rectangular areas of approximately two speckles in size were defined on nerve fiber bundles. The defined area was then treated as a subimage and a series of such subimages were derived from the original full images. To compensate for possible tissue shift during the measurement, the entire set of images was registered by horizontal and vertical translation.

A correlation function was used to analyze the dynamic change of speckle patterns on bundles.[12] In this method, any

subimage in an image series was chosen as a reference image. CCs between the reference subimage and each consecutive subimage in the image series were calculated as

$$CC_I = \frac{\sum_m \sum_n (A_{mn} - \bar{A})(I_{mn} - \bar{I})}{\sqrt{\left[\sum_m \sum_n (A_{mn} - \bar{A})^2\right]\left[\sum_m \sum_n (I_{mn} - \bar{I})^2\right]}} \quad (4)$$

where A_{mn} was the intensity of the mth row and nth column element in the reference subimage with a typical value of seven to nine for m and n, $\bar{A}$ was the mean intensity of the A_{mn}, and I represented the Ith subimage in the image series.[29] A high CC indicates high similarity between two images. CC equals one for identical images. CC_I was calculated for each subimage and plotted against time. The CC time course was then fitted with an exponential function, and the time constant (τ) of the function was used as a measure of the rate of change of speckle.

The same analysis was also applied to a nearby gap, a retinal area between bundles.

Results

Speckle Phenomena in RNFL Reflectance

In reflectance images, retinal nerve fiber bundles appeared as bright stripes against a darker background. Figure 1A is a reflectance image of a normally prepared retina at 660 nm. Reflectance within bundles was not uniform; rather, bright pixels clustered to form a speckled texture as shown in a magnified view of the bundles (Fig. 1B). Speckles were randomly distributed within the bundles with a speckle size of approximately 3 pixels wide.

One characteristic of reflectance speckle is its dependence on wavelength.[14,15,19] Figures 1C–F show the same bundles in Figure 1B imaged at different wavelengths. At a short wavelength (440 nm), bundles appeared smooth; speckles were hardly perceivable. With increase of wavelength, the speckled texture became more apparent with increasing contrast; Figure 1F shows that at 830 nm, bright pixels clustered to form high-contrast speckles. Note that all images in Figure 1 had the same exposure duration of 2 seconds.

Temporal Change of RNFL Reflectance Speckle

In normally prepared retina, the speckle pattern was not stationary. Within a short period, speckled texture was similar and then slowly changed its pattern over time. Figures 2A–D show reflectance images taken at different time intervals. To appreciate the changes of speckled texture, Figures 2E–G demonstrate difference in images between Figures 2B–D and Figure 2A, respectively. In the difference image with a 5-second interval (Fig. 2E), bundle boundaries were hardly discernible, suggesting that the two images were similar. However, with the increase of imaging interval, bundles became more apparent (Figs. 2F, 2G) due to the change of the speckle pattern within the bundles. In contrast, the difference in gap areas looked smoother than that of the bundles and was similar in Figures 2E–G, which indicates that the reflectance of gap areas varied little between images.

In time-lapse movies of RNFL reflectance images, the speckled texture of normally prepared retinas was seen to change with time, with individual speckles fading in and out, as demonstrated by Supplementary Movie S1. The speckles did not appear to move along bundles. There were some spots (three circled) that maintained fairly constant brightness. These were located on a blood vessel running parallel to the nerve fiber bundles. In contrast to normally prepared retinas, the speckled texture of the RNFL in retinas fixed with paraformaldehyde did not show apparent change with the lapse of time (Supplementary Movie S2). To quantitatively assess the similarity of a speckled pattern over time, a correlation analysis was applied to an image series. Figure 3A shows the time course of the CC of a series of subimages that sampled approximately two speckles on a bundle in the normally prepared retina shown in Supplementary Movie S1 (black box in Fig. 3C). The CC was high at the beginning of the image series, but decreased gradually with time and after approximately 2 minutes reached a plateau. In contrast, the CC time course of a nearby gap area (Fig. 3B) shows that CC decreased immediately to a plateau. Fitting an exponential function gave $\tau = 0.38$ and $\tau = 0.08$ minutes for the bundle and gap areas, respectively. Twelve bundles from five normally prepared retinas show similar results with $\tau = 0.56 \pm 0.26$ minutes (mean $\pm$ SD) and ranging from 0.28 to 1.17 minutes. For the 12 corresponding gap areas $\tau = 0.09 \pm 0.11$ minutes, which was significantly lower than that of the bundle areas ($P < 0.001$).

The gradual decrease of CC of bundle speckles suggests that temporal change of speckle texture was associated with gradual changes in the position of reflecting structures within axons, or axonal dynamic activity. To test this hypothesis, image series were taken on four retinas in which structural positions were fixed with paraformaldehyde. The reflectance images of fixed nerve fiber bundles exhibited a speckled texture similar to unfixed retina (Fig. 3F); however, the speckle patterns did not vary with time as shown in a time-lapse movie (Supplementary Movie S2). Quantitatively, Figure 3D shows high values of CC over the entire time period. In contrast, the

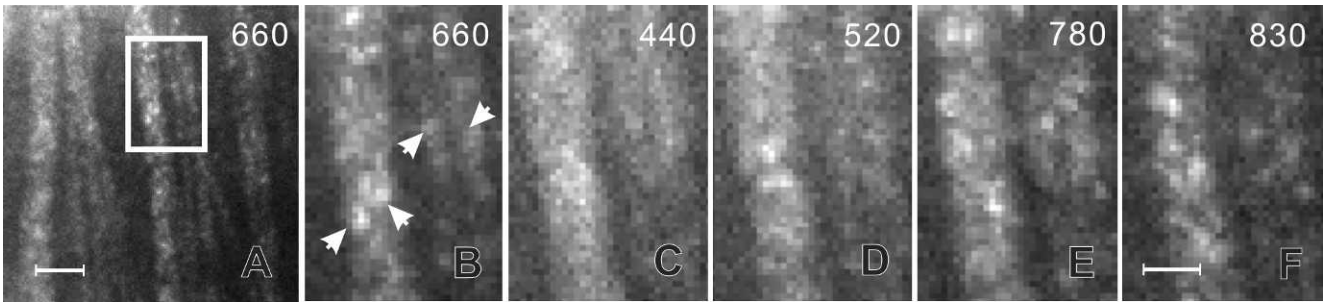

Figure 1. Speckle of RNFL reflectance and its wavelength-dependence. (**A**) Reflectance image taken at 660 nm showing bright bundles against a darker background; bundles are granular looking. (**B–F**) Magnified view of the bundles outlined in (**A**). *Arrows* in (**B**) show individual speckles at 660 nm. At 440 nm (**C**) bundles appear smooth; however, with increase of wavelength (**D–F**), the speckled texture becomes more apparent. The *gray scales* of (**B**) to (**F**) are the same. *Scale bars*: 50 μm (**A**) and 20 μm (**B–F**).

Investigative Ophthalmology & Visual Science

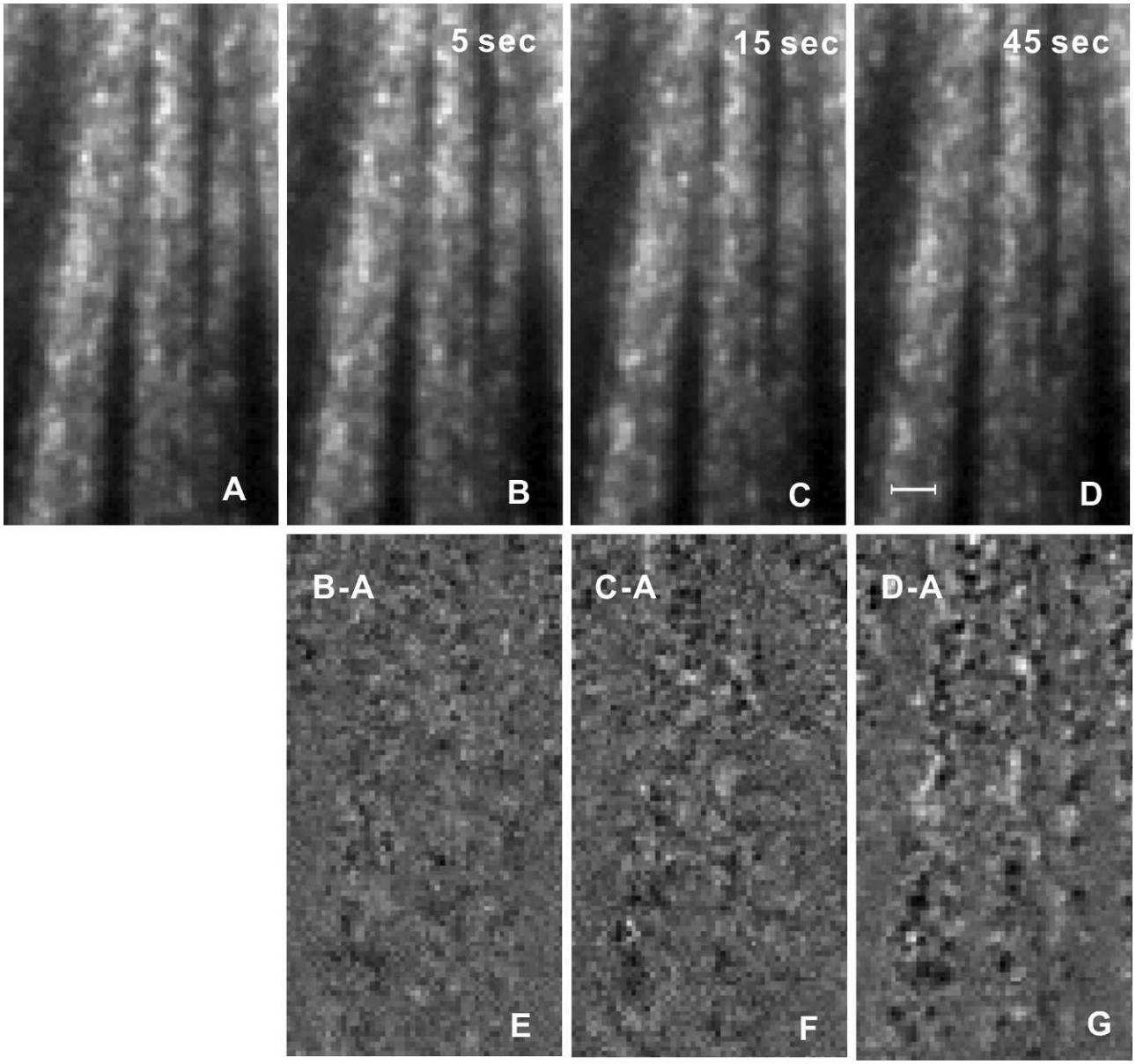

Figure 2. Temporal change of speckled texture. (**A–D**) Reflectance images taken at 660 nm with different imaging intervals. (**E–G**) Difference in images between (**B**) to (**D**) and (**A**). Bundle boundaries become more apparent with increase of imaging interval. *Scale bar*: 20 μm. The *gray scales* of (**A**) to (**D**) and (**E**) to (**G**) are the same.

CC time course of nearby gaps (Fig. 3E) was similar to that of unfixed tissue (Fig. 3B).

To rule out that the change observed in our experiments was due to circulation of the physiological solution, image series of normally prepared retinas were taken with the circulation of the physiological solution halted. The gradual change of speckle pattern persisted. To further confirm that the detected change of speckle did not arise from tissue movement, two fixed retinas were purposely moved by 10 to 250 μm laterally or 5 μm to 100 μm in depth with the light source and camera positions unchanged. After image registration to compensate for the tissue movement, the CC of subimages on nerve fiber bundles randomly varied from 0.88 to 0.95 and was not correlated with the amount of tissue shift.

RNFL Speckle in Retinas Treated With Low Temperature and MT Depolymerization

Two schemes were designed to further test the hypothesis that the temporal change of RNFL reflectance speckle was associated with axonal dynamic activity. In the first, we lowered the temperature of the physiologic solution from 34°C to 24°C, with the expectation that lower temperature would slow axonal transport.[30] In two retinas, an image series was obtained at 34°C followed by another at 24°C. The results from one of these retinas are shown in Figure 4. At 34°C, the change in speckle was similar to other retinas, with $\tau = 0.38$ min. At 24°C, however, the change in speckle slowed by a factor of nearly three to $\tau = 1.11$ minutes. In the second retina $\tau = 0.27$ minutes at 34°C and 0.72 minutes at 24°C. A third retina was measured at 24°C only; three bundles gave values of $\tau =$ 0.90, 1.03, and 1.13 minutes. A one-way analysis of variance

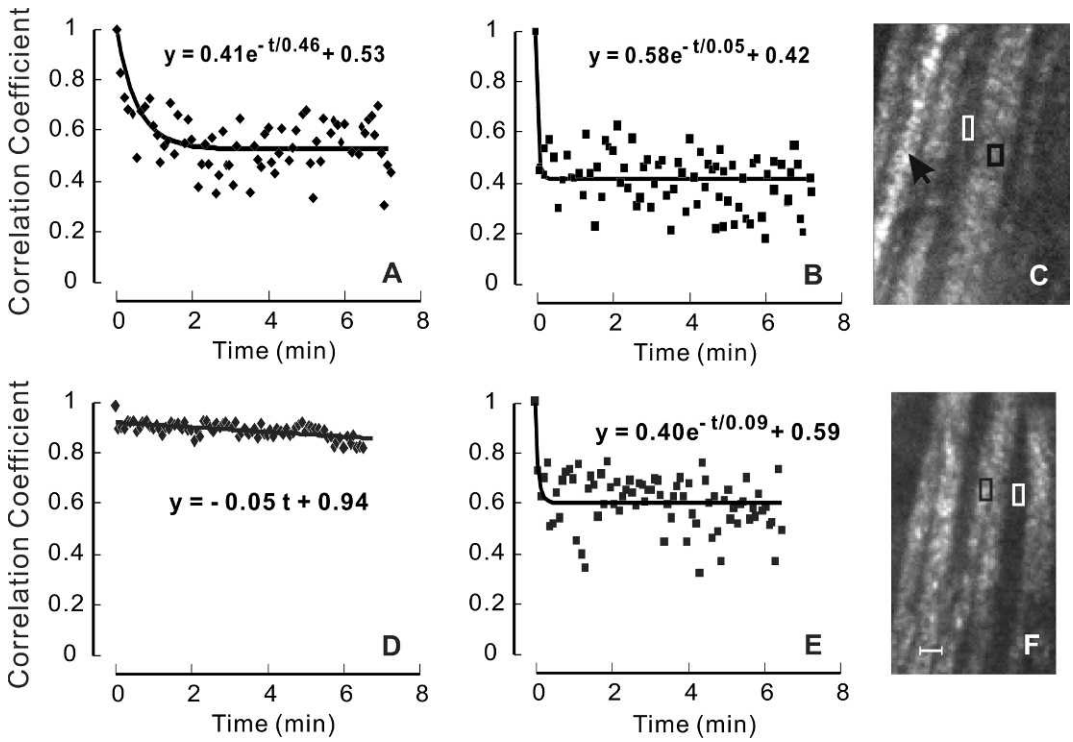

Figure 3. CC time courses of normally prepared (**A**–**C**) and fixed retinas (**D**–**F**). (**A**) CC of a bundle area sampling two speckles in a normally prepared retina, showing exponential decrease of CC with time. (**D**) CC of a bundle area in a fixed retina, showing highly correlated speckled pattern over time. (**B**, **E**) CC of the gap areas in (**C**) and (**F**), respectively, decrease sharply at the beginning of the image series and then vary around a constant. Exponential function fit for (**A**, **B**) and (**E**); linear function fit for (**D**). (**C**, **F**) The appearance of the speckled texture in the normally prepared (**C**) and fixed (**F**) retinas was similar. *Black arrow*: blood vessel. *Black* and *white boxes*: bundle and gap areas for the plots in (**A**, **D**) and (**B**, **E**), respectively. *Scale bar*: 20 μm.

showed that in the five bundles of the three retinas measured at 24°C, τ was significantly higher than that measured at 34°C ($P = 0.003$).

We also used colchicine to depolymerize MTs. Because MTs are an active cytostructure participating in axonal transport and also a major contributor to RNFL reflectance,[21–25,31] we postulated that depolymerization of MTs would hamper axonal transport and thereby reduce temporal change of RNFL reflectance speckle. Figure 5A demonstrates a CC time course before colchicine treatment with $\tau = 0.24$ minute. After 15 minutes of treatment, the decrease of CC became slower with $\tau = 0.87$ minute (Fig. 5B), whereas with 50 minutes of treatment the decay became much slower ($\tau = 2.85$ minutes; Fig. 5C).

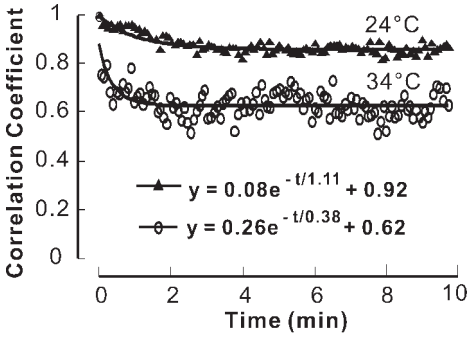

Figure 4. Effect of physiologic solution temperature on temporal change of RNFL speckle. *Circles*: a typical CC time course of a retina perfused at 34°C; *triangles*: a CC time course of the same retina perfused at 24°C. Low perfusion temperature results in a larger time constant.

However, at this time point, speckles were still apparent in the reflectance image (Fig. 5D). The CC time course of nearby gaps was similar over the entire treatment period (not shown). Six bundles in four treated retinas showed that τ increased from 0.55 ± 0.25 minute at the baseline period to 1.34 ± 0.80 minutes and 2.39 ± 0.63 minutes after colchicine treatment of approximately 15 to 20 minutes and 40 to 50 minutes, respectively. A paired *t*-test for means showed that τ increased significantly with the colchicine treatment ($P = 0.04$ with 15–20 minutes of treatment and $P = 0.001$ after 45 minutes of treatment).

Discussion

High resolution reflectance images of nerve fiber bundles in the RNFL exhibit a speckled texture at long wavelengths that becomes less apparent at short wavelengths (Fig. 1). This appearance may be understood by considering the size of a coherence volume relative to the RNFL thickness. Figure 6 shows schematic drawings of the approximately cylindrical coherence volumes produced by the IMR and calculated with Equations 2 and 3. With quasi-monochromatic illumination from an incandescent source, reflectance speckle arises mostly from temporal interference, that is, interference between scattered components of a wave and itself delayed in depth. At 660 nm, the coherence length is comparable to the thickness of a typical nerve fiber bundle (~15 μm) and rays scattered from throughout a bundle contribute to the speckled texture. At 440 nm, however, the coherence length is only a fraction of the bundle thickness and the resulting speckles from different depths are superimposed on the average reflectance. Short-wavelength speckles, therefore, have lower contrast, as seen in

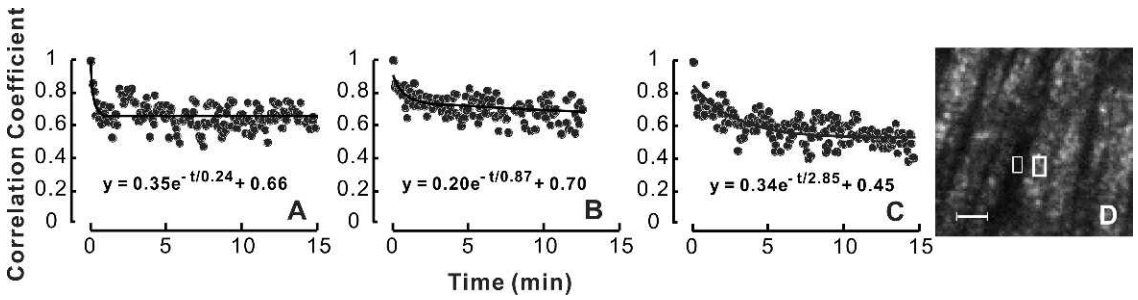

Figure 5. Effect of MT depolymerization on temporal change of RNFL reflectance speckle. (**A**) Ten minutes before colchicine treatment; (**B**, **C**) 15 and 50 minutes, respectively, after colchicine treatment. Colchicine treatment causes slow decay of CC. (**D**) Reflectance image corresponding to the time point in (**C**); the speckled texture was still present. *White boxes*: bundle and gap areas. *Scale bar*: 30 μm.

Figure 1C. In this view of the origin of RNFL reflectance speckle, the speckle pattern is a property of the RNFL, associated with its internal structure. To demonstrate this concept and to rule out a possible contribution of tissue movement to the change of speckled texture, we used fixed retinas and purposely shifted the retina laterally and in depth. These movements caused little change in the speckled texture of the RNFL, confirming that the speckles were a property of the tissue itself and not of its position in the optical system.

The speckled texture of RNFL reflectance images was studied at 660 nm. A time-lapse image series showed that the speckle pattern changed over a period of a few minutes. The speckles appeared and faded but did not move along bundles. We quantified the change in a series of subimages with CCs between the initial and subsequent speckle patterns, which provided a measure of their similarity. For normally prepared retinas in conditions designed to maintain physiological activity, the CC was high at the beginning of an image series, indicating similarity between the speckle patterns. With the lapse of time, the CC decreased gradually until after a few minutes it varied around a plateau determined by features common to all subimages. The time constant of an exponential fit to the decrease was used to quantify the rate of change of CCs. Fixation of tissue structure with paraformaldehyde did not affect the qualitative appearance of the RNFL speckle, but eliminated the temporal change, suggesting that speckle dynamics resulted from temporal change of reflecting structures.

Compared with the gradual decrease of CCs in bundle areas, the CC of gap areas decreased abruptly to a plateau. The average $\tau = 0.09$ minute was approximately the interval used for collecting an image series. The result suggests that the reflectance of gap areas was not correlated between two consecutive images and reflectance at each pixel changed randomly. The time courses of CCs in gaps were similar for unfixed and fixed retinas, suggesting that the random change of gap reflectance was due to the noise of the optical measurements.

Consideration of structural change within axons immediately suggests a role for axonal transport. Axonal transport is achieved by the binding of molecules, vesicles, and organelles (so-called cargo) to molecular motors that generate movement along the axons.[20] A direct role for axonal transport as the source of the temporal change in speckle is problematic, however, because the structures that scatter light in the RNFL are known to be cylinders oriented along the axon bundles,[28] with approximately half the reflectance coming from MTs.[25,26] We hypothesize that movement in depth of scattering structures occurs as a secondary consequence of axonal transport. Figure 7 depicts a possible biophysical model for this concept. The model in Figure 7 shows the component of transport that uses MTs as tracks. In this model, the movement of the motor-cargo complexes along MTs changes the spacing between MTs and hence the relative phase of the reflected light. Within a coherence volume as depicted in Figure 6, these phase changes sum coherently to produce a spatial change in the speckle pattern without movement along bundles. Although Figure 7 explicitly shows MTs, other cylindrical scattering structures could be similarly displaced by axonal transport and contribute to speckle dynamics. Further, other displacement mechanisms could be involved, and a more general hypothesis would link speckle change to unspecified axonal dynamic activity.

To test the hypothesis that temporal change of RNFL reflectance speckle is associated with axonal dynamic activity, we performed three experiments expected to alter this activity. The first, mentioned above, was tissue fixation, which resulted in the speckle pattern becoming highly correlated over time (Fig. 3D). The second experiment used normally prepared retinas perfused with a physiologic solution at a lower temperature. Because low temperature slows axonal transport[30] and other physiological processes, the slower decay of the CC measured at 24°C (Fig. 4) demonstrates a link between change of speckle and axonal dynamic activity. The third experiment attempted to relate temporal change of RNFL speckle to axonal transport by depolymerizing MTs with

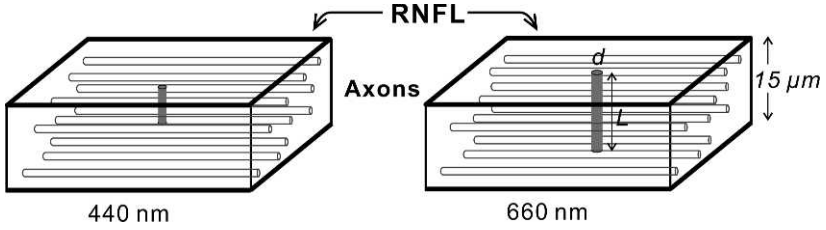

Figure 6. Schematic of coherence volumes in the RNFL. Rays scattered at points within a coherence volume (*gray cylinder*) can produce interference effects. The size of a coherence volume increases with increasing wavelength. At 440 nm, $L = 6$ μm and $d = 1.4$ μm; at 660 nm, $L = 14$ μm and $d = 2.1$ μm.

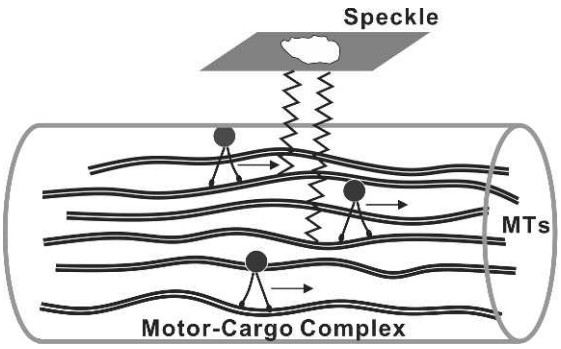

FIGURE 7. Biophysical model of RNFL reflectance speckle. Axonal MTs, an important contributor to RNFL reflectance, act as tracks to guide motor-cargo complexes along axons. In this model, longitudinal movement of the complexes changes the spacing between MTs and thus the location in depth of the scattering structures. The change in relative phases within each coherence volume results in a change of speckle texture.

colchicine. MTs are a key cytostructure for transferring proteins and cellular components along the axons,[21–23] and MT depolymerization was expected to disrupt axonal transport.[32] The CC time courses (Fig. 5) obtained with different durations of MT depolymerization confirmed this expectation; the decay of CC became slower with the colchicine treatment and the time constant increased with the duration of treatment.

Change of axonal transport is often an early sign in many optic neuropathic diseases, such as glaucoma.[33–40] Optical assessment of RNFL is currently limited to evaluating RNFL structure. This study demonstrated that change of RNFL reflectance speckle reveals axonal dynamic activity, perhaps axonal transport. This new concept may allow a novel approach for assessing the RNFL, namely, detecting physiological activity of axons, which may precede loss of axonal structure.

This study used an in vitro preparation of retina to eliminate the confounding effects of other ocular tissues on measurements. Recently reported RNFL images obtained with adaptive optics scanning laser ophthalmoscopy (AOSLO) reveal a similar speckled texture of RNFL reflectance in human eyes (Scoles DH, et al. *IOVS* 2012;53:ARVO E-Abstract 6954).[41] If it can be demonstrated that the apparent AOSLO speckle also arises from interference, it may be possible to adapt AOSLO technology for noninvasive assessment of axonal dynamic activity in clinical practice.

Acknowledgments

Supported by National Institutes of Health Grant R01-EY019084, National Institutes of Health Core Grant P30-EY014801, a Department of Defense Career Development Award (DOD Grant W81XWH-09-1-0675), and an unrestricted grant from Research to Prevent Blindness, Inc.

Disclosure: **X.-R. Huang**, None; **R.W. Knighton**, None; **Y. Zhou**, None; **X.-P. Zhao**, None

References

1. Schuman JS, Hee MR, Arya AV, et al. Optical coherence tomography: a new tool for glaucoma diagnosis. *Curr Opin Ophthalmol*. 1995;6:89–95.
2. Medeiros FA, Bowd C, Zangwill LM, Patel C, Weinreb RN. Detection of glaucoma using scanning laser polarimetry with enhanced corneal compensation. *Invest Ophthalmol Vis Sci*. 2007;48:3146–3153.
3. Alexandrescu C, Dascalu A, Panca A, et al. Confocal scanning laser ophthalmoscopy in glaucoma diagnosis and management. *J Med Life*. 2010;3:229–234.
4. Cense B, Chen TC, Park BH, Pierce MC, De Boer JF. Thickness and birefringence of healthy retinal nerve fiber layer tissue measured with polarization sensitive optical coherence tomography. *Invest Ophthalmol Vis Sci*. 2004;45:2606–2612.
5. Huang X-R, Bagga H, Greenfield DS, Knighton RW. Variation of peripapillary retinal nerve fiber layer birefringence in normal human subjects. *Invest Ophthalmol Vis Sci*. 2004;45:3073–3080.
6. Huang X-R, Knighton RW. Microtubules contribute to the birefringence of the retinal nerve fiber layer. *Invest Ophthalmol Vis Sci*. 2005;46:4588–4593.
7. Fortune B, Wang L, Cull G, Cioffi GA. Intravitreal colchicine causes decreased RNFL birefringence without altering RNFL thickness. *Invest Ophthalmol Vis Sci*. 2008;49:255–261.
8. Huang X-R, Zhou Y, Kong W, Knighton RW. Reflectance decreases before thickness changes in the retinal nerve fiber layer in glaucomatous retinas. *Invest Ophthalmol Vis Sci*. 2011;52:6737–6742.
9. Dwelle J, Liu S, Wang B, et al. Thickness, phase retardation, birefringence, and reflectance of the retinal nerve fiber layer in normal and glaucomatous non-human primates. *Invest Ophthalmol Vis Sci*. 2012;53:4380–4395.
10. van der Schoot J, Vermeer KA, de Boer JF, Lemij HG. The effect of glaucoma on the optical attenuation coefficient of the retinal nerve fiber layer in spectral domain optical coherence tomography images. *Invest Ophthalmol Vis Sci*. 2012;53:2424–2430.
11. Vermeer KA, van der Schoot J, Lemij HG, de Boer JF. RPE-normalized RNFL attenuation coefficient maps derived from volumetric OCT imaging for glaucoma assessment. *Invest Ophthalmol Vis Sci*. 2012;53:6102–6108.
12. Aizu Y, Asakura T. Bio-speckle phenomena and their application to the evaluation of blood flow. *Optics and Laser Technology*. 1991;23:205–219.
13. Schmitt JM, Xiang SH, Yung KM. Speckle in optical coherence tomography. *J Biomed Opt*. 1999;4:95–105.
14. Boas DA, Dunn AK. Laser speckle contrast imaging in biomedical optics. *J Biomed Opt*. 2010;15:1–12.
15. Briers JD. Laser Doppler, speckle and related techniques for blood perfusion mapping and imaging. *Physiol Measur*. 2001;22:R35–R66.
16. Nagahara M, Tamaki Y, Tomidokoro A, Araie M. In vivo measurement of blood velocity in human major retinal vessels using the laser speckle method. *Invest Ophthalmol Vis Sci*. 2011;52:87–92.
17. Qiu J, Li P, Luo W, Wang J, Zhang H, Luo Q. Spatiotemporal laser speckle contrast analysis for blood flow imaging with maximized speckle contrast. *J Biomed Opt*. 2010;15:0160031–0160035.
18. Briers JD, Fercher AF. Retinal blood-flow visualization by means of laser speckle photography. *Invest Ophthalmol Vis Sci*. 1982;22:255–259.
19. Knighton RW, Huang X-R. Visible and near-infrared imaging of the nerve fiber layer of the isolated rat retina. *J Glaucoma*. 1999;8:31–37.
20. Darnell J, Lodish H, Baltimore D. *Molecular Cell Biology*. New York: Scientific American Books; 1990.
21. Morgan JE. Circulation and axonal transport in the optic nerve. *Eye*. 2004;18:1089–1095.
22. Susalka SJ, Pfister KK. Cytoplasmic dynein subunit heterogeneity: implications for axonal transport. *J Neurocytol*. 2000;29:819–829.
23. Muresan V. One axon, many kinesins: what's the logic? *J Neurocytol*. 2000;29:799–818.

24. Knighton RW, Huang X-R, Zhou Q. Microtubule contribution to the reflectance of the retinal nerve fiber layer. *Invest Ophthalmol Vis Sci*. 1998;39:189–193.
25. Huang X-R, Knighton RW, Cavuoto LN. Microtubule contribution to the reflectance of the retinal nerve fiber layer. *Invest Ophthalmol Vis Sci*. 2006;47:5363–5367.
26. Karu TI. Low power laser therapy. In: Tuan V-D, ed. *Biomedical Photonics Handbook*. Boca Raton, FL: CRC Press; 2003:1–48.
27. Born M, Wolf E. *Principles of Optics: Electromagnetic Theory of Propagation, Interference, and Diffraction of Light*. Cambridge, UK: Cambridge University Press; 1999.
28. Knighton RW, Huang X-R. Directional and spectral reflectance of the rat retinal nerve fiber layer. *Invest Ophthalmol Vis Sci*. 1999;40:639–647.
29. MatLab Image Processing Toolbox Documentation. Available at: http://www.Mathworks.Com/help/images/ref/corr2.html. Accessed March 1, 2012.
30. Edstrom A, Hanson M. Temperature effects on fast axonal transport of proteins in vitro in frog sciatic nerves. *Brain Res*. 1973;58:345–54.
31. Goode BL, Drubin DG, Bames G. Functional cooperation between the microtubule and actin cytoskeletons. *Curr Opin Cell Biol*. 2000;12:63–71.
32. Tang-Schomer MD, Johnson VE, Baas PW, Stewart W, Smith DH. Partial interruption of axonal transport due to microtubule breakage accounts for the formation of periodic varicosities after traumatic axonal injury. *Exp Neuro*. 2012; 233:364–372.
33. Quigley HA, McKinnon SJ, Zack DJ, et al. Retrograde axonal transport of BDNF in retinal ganglion cells is blocked by acute IOP elevation in rats. *Invest Ophthalmol Vis Sci*. 2000;41: 3460–3466.
34. Saleb M, Nagaraju M, Porciatti V. Longitudinal evaluation of retinal ganglion cell function and IOP in the DBA/2J mouse model of glaucoma. *Invest Ophthalmol Vis Sci*. 2007;48:4564–4572.
35. Buckingham BP, Inman DM, Lambert W, et al. Progressive ganglion cell degeneration precedes neuronal loss in a mouse model of glaucoma. *J Neurosci*. 2008;28:2735–2744.
36. Morfini GA, Burns M, Binder LI, et al. Axonal transport defects in neurodegenerative diseases. *J Neurosci*. 2009;29:12776–12786.
37. Baltan S, Inman DM, Danilov CA, Morrison RS, Calkins DJ, Horner PJ. Metabolic vulnerability disposes retinal ganglion cell axons to dysfunction in a model of glaucomatous degeneration. *J Neurosci*. 2010;30:5644–5652.
38. North RV, Jones AL, Drasdo N, Wild JM, Morgan JE. Electrophysiological evidence of early functional damage in glaucoma and ocular hypertension. *Invest Ophthalmol Vis Sci*. 2010;51:1216–1222.
39. Salinas-Navarro M, Alarcon-Martinez L, Valiente-Soriano RJ, et al. Ocular hypertension impairs optic nerve axonal transport leading to progressive retinal ganglion cell degeneration. *Exp Eye Res*. 2010;90:168–183.
40. Crish SD, Calkins DJ. Neurodegeneration in glaucoma: progression and calcium-dependent intracellular mechanisms. *Neuroscience*. 2011;176:1–11.
41. Takayama K, Ooto S, Hangai M, et al. High-resolution imaging of the retinal nerve fiber layer in normal eyes using adaptive optics scanning laser ophthalmoscopy. *PLoS One*. 2012;7: e33158.

Investigative Ophthalmology & Visual Science